

Discovering A Variety of Objects in Spatio-Temporal Human-Object Interactions*

Yong-Lu Li^{1†}, Hongwei Fan^{2†}, Zuoyu Qiu¹, Yiming Dou¹, Liang Xu¹, Hao-Shu Fang¹,
 Peiyang Guo¹, Haisheng Su², Dongliang Wang², Wei Wu², Cewu Lu^{1‡}

¹Shanghai Jiao Tong University, ²Sensetime

{yonglu.li, 17803091056, douyiming, lucewu}@sjtu.edu.cn

{fanhongwei1, suhaisheng, wangdongliang, wuwei}@senseauto.com, {liangxuy96, fhaoshu}@gmail.com
 {helllobrian18}@163.com

Abstract

*Spatio-temporal Human-Object Interaction (ST-HOI) detection aims at detecting HOIs from videos, which is crucial for activity understanding. In daily HOIs, humans often interact with a variety of objects, e.g., holding and touching dozens of household items in cleaning. However, existing whole body-object interaction video benchmarks usually provide limited object classes. Here, we introduce a new benchmark based on AVA: **Discovering Interacted Objects (DIO)** including 51 interactions and 1,000+ objects. Accordingly, an ST-HOI learning task is proposed expecting vision systems to track human actors, detect interactions, and simultaneously discover interacted objects. Even though today's detectors/trackers excel in object detection/tracking tasks, they cannot localize diverse/unseen objects in DIO well. This profoundly reveals the limitation of current vision systems and poses a great challenge. Thus, how to leverage spatio-temporal cues to address object discovery is explored, and a baseline **Hierarchical Probe Network (HPN)** is devised to discover interacted objects utilizing hierarchical spatio-temporal human/context cues. In extensive experiments, HPN demonstrates decent performance. Data and code are available at <https://github.com/DirtyHarryLYL/HAKE-AVA>.*

1. Introduction

As the prototypical unit of human activities, human-object interaction (HOI) plays an important role in activity understanding. Recently, image-based HOI learning [6, 23, 56, 41, 49, 73, 19] achieves great progress. However, daily HOIs may need temporal cues to avoid ambiguity in detection, e.g., *pick_up-cup* and *put_down-cup*. Thus,

*Technical report. A part of the **HAKE** project. HAKE also provides human body Part States (PaSta) labels [44] paired with DIO on AVA.

†The first two authors contribute equally.

‡Corresponding author.

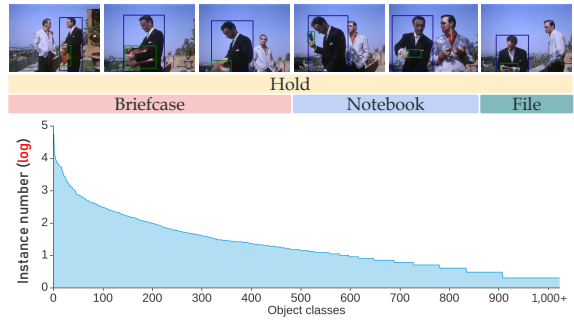


Figure 1: Object diversity of DIO. In daily HOIs, we often interact with many objects. DIO is rich in object classes and severely long-tailed, thus is more challenging.

many video HOI works [11, 70, 84, 29, 82, 61, 52, 34, 55] are proposed to advance spatio-temporal HOI (ST-HOI) learning.

HOI data is often long-tailed, *i.e.*, some HOIs are much more common than rare ones, which imports great challenges to vision systems [6, 27]. Generally, HOI is depicted as $\langle \text{human}, \text{verb}, \text{object} \rangle$ triplet. As the subjective is always human, thus rare HOIs are usually imported from rare verbs or objectives. For rare verbs, few-shot action learning has been studied in many works [6, 30, 27], but the rare objective problem is previously overlooked. In daily HOIs, we usually perform **limited** actions upon a variety of objects. For example, in Fig. 1, a person *holds* three different objects in a very short time. But many video HOI datasets [64, 70, 29] contain few object classes, *e.g.*, Charades [64], DALY [70], Action Genome [29] all have less than 50 classes (Tab. 1). This makes vision systems built upon them lack the ability to localize various objects. For another, some video HOI datasets [11, 52, 61] including diverse objects are proposed recently, *e.g.*, EPIC-Kitchens [11] contains 323 classes, Something-Else [52] includes 18 K uncurated classes, 100DOH [61] provides 110.1 K objects of unknown class. However, they all focus on *hand-object* interactions and *first-view* videos (100DOH [61] also has *third-view* videos). As **whole body-object** interaction detection

from **third-view** videos matters to numerous applications (*e.g.*, service robots, health-care), we prefer to study third-view body-object interactions, such as *ride/sit on* (chair, horse, *etc.*), *enter/exit* (train, bus, *etc.*). In this work, we propose a large-scale third-view ST-HOI benchmark building upon AVA [27]: **Discovering Interacted Objectives (DIO)**. It contains 51 interactions and **1,000+** object classes to afford HOI learning including many rare/unseen objects. And **290** K object boxes in **290** K \langle human, verb, object \rangle frame-level triplets are provided.

Accordingly, an ST-HOI learning task and a corresponding integrated metric are proposed, requiring visual systems to track human actors and detect interactions while localizing interacted objects simultaneously. Notably, entity-relationship detection [62, 6, 42] often assumes that object locations can be obtained beforehand via detection [58]/tracking [53]. But this is difficult considering the diverse interacted object classes (Fig. 1). In our task, object discovery is seen as *important* and *exploratory* as interaction detection. To this end, we split DIO to make its test set contain numerous *rare* ST-HOI triplets composed of *seen* interactions and *rare/unseen* objects. Since few/zero-shot object detection [1] is still an open problem, current vision systems would struggle. For example, cutting-edge image/video detectors [58, 9] finetuned on our train set all achieve less than 20 AP. Hence, the exploration of **interacted object discovery** in DIO is extremely challenging but essential as the touchstone for the deep learning paradigm.

To tackle ST-HOI learning, we study how to track human actors, detect interactions and discover various objects with multiple points of view (Sec. 5) and propose a baseline system **Hierarchical Probe Network (HPN)**. It leverages a *hierarchical-probe* policy to discover objects. Hierarchical-probe indicates that utilizing the spatio-temporal cues hierarchically, such as from *local human parts*, to *whole human body* and *global context*, to discover possible interacted objects (Sec. 4). In extensive experiments, HPN achieves impressive performance. However, DIO remains challenging and the three sub-tasks still have lots of room for improvement. We believe DIO would inspire a new line of studies and pose new challenges and opportunities for the development of deeper activity understanding.

Our contributions are three-fold: (1) We propose a large-scale third-view ST-HOI benchmark DIO, including 299 videos, 51 interactions, and 1,000+ objects. (2) A novel ST-HOI learning task and its metric are proposed to drive the studies on finer-grained activity parsing and understanding. (3) Accordingly, a baseline system, Hierarchical Probe Network (HPN), is proposed and achieves impressive performance on DIO.

2. Related Works

Object Tracking. Object tracking is an active field and has two main branches, *i.e.*, Single-Object Tracking (SOT) [10, 15] and Multi-Object Tracking (MOT) [53, 59, 3]. Recently, tracking-by-detection (TBD) [31, 60] receives lots of attention and achieves state-of-the-art performance. As our main goal is object discovery, we directly adopt the cutting-edge DeepSORT [71] and FairMOT [80] as human trackers.

Human-Object Interaction (HOI). In terms of image-based HOI learning, both image-level [7, 30] and instance-level [6, 23, 45, 25, 41, 43, 20, 48, 40, 39] methods achieve successes with the help of large-scale datasets [6, 7, 44, 42]. As for HOI learning from third-view videos, recently many large-scale datasets [27, 64, 70, 29, 61, 22, 4] are released to promote this field, thus providing a data basis for us. They provide clip-level [4, 22, 64] or instance-level [27, 29, 70] action labels, but few of them [22, 64, 70, 29] afford diverse object classes. Though some datasets [52, 11] provide instance labels of diverse object classes, they usually concentrate on egocentric hand-object interaction understanding [75]. Relatively, we choose to focus on whole body-object interaction learning based on third-view videos and propose DIO featuring the discovery of diverse objects. Recently, there are also many methods studying video-based visual relationship [62, 47, 68] and HOI [82, 56, 69, 51, 2, 24].

Object Detection. Object detection [58, 57] achieves huge success along with the development of deep learning and large-scale datasets [46], but they may struggle without enough training data. Thus, some works [16, 1] start to study few/zero-shot detection. Moreover, as videos can provide temporal cues of moving objects, video object detection [9] also receives attention recently. Different from typical detection, some studies try to utilize context cues, such as human actor [32, 25], action recognition [77, 76], object relation [28], to advance object localization. Gkioxari et al. [25] treat object localization as density estimation and use a Gaussian function to predict object location. Kim et al. [32] borrow cues from human pose and language prior to constructing a weakly-supervised detector. In this work, we tackle object discovery via hierarchical perspectives, *i.e.*, local human part, human, and global context.

3. Constructing DIO

Data Collection. To support practical ST-HOI learning, we collect third-view videos from large-scale dataset AVA [27]. It contains 430 videos with spatio-temporal labels of 80 atomic actions (body motions and HOIs). As AVA includes complex HOIs in diverse scenes, it can bring great visual diversity to our benchmark. We extract the HOI-related frames and the corresponding human boxes and action la-

belts, thus the clips in DIO have uneven temporal durations. Notably, we only consider the non-human objectives in HOIs. Overall, based on the available train and validation (val) sets of AVA 2.2 [27] (299 videos), we choose 74 hours of video including 51 HOIs (detailed in the supplementary).

Object Annotation. AVA provides labels with a stride of 1 second, so we add boxes and class labels for all interacted objects with the same stride. **First**, as a human can perform multi-interaction simultaneously, we set the annotating unit as a clip including one *single* interaction. For example, a 30s clip including an actor *holds-sth* (1-30s) and *inspects-sth* (10-15s), will be divided into two sub-clips, *i.e.*, a 30s sub-clip for *holds-sth* and a 5s sub-clip for *inspects-sth*. In brief, each sub-clip contains **one** verb and **one/several** class-agnostic interacted objects. Then, sub-clips are annotated separately, and each one is annotated by at least 3 annotators and checked by an expert to ensure quality. **Second**, as AVA contains various scenarios and diverse objects, to better locate objects and avoid ambiguity, each annotator is given a whole sub-clip to draw boxes and classify them. In default, we use COCO [46] 80 objects as a class pool. If annotators think an object is not in the pool, they are asked to input a suitable class according to their judgments. If an object cannot be recognized, they can choose the “unknown” option, but the “unknown” ratio is controlled by our annotation tool. Finally, we find that surprising 42.66% of object instances are beyond our pool. **Third**, after exhaustive annotation, we fix the input typos, exclude outliers via clustering, and combine similar items. After cleaning, **1,000+** classes are extracted. We then conduct re-recognition for the frames including “unknown” objects. Finally, only 7,476 frames (2.57%) still contain “unknown”, due to the blur frames or too small objects. Fig. 2 (a) shows the object class composition according to WordNet [54]. For more details about classes please refer to our supplementary.

New Challenge. Notably, the class labels are used for analysis instead of evaluation here, as current detectors [58, 57, 9] cannot detect such an amount of classes. For example, a recent large-scale dataset FSOD [16] only includes **20.85%** of our classes. And for practical applications, class-agnostic interacted object discovery is also essential for HOI learning, taking the situation in Fig. 1 as an example. Hence, in our train set, 328 object classes only have less than 5 samples (boxes), and 98 classes are **unseen** in the testing. As few/zero-shot detection is beyond the scope of our work, we leave the opportunity of a more difficult setting including object classification to future work.

ST-HOI Tracklet. Since one human may interact with multi-object via multi-interaction simultaneously, we largely decrease the complexity via the above sub-clip segmentation to decouple interactions. Next, to generate the ST-HOI labels, we further consider the objects in each sub-

Dataset	Frames	Actions	Objects		HOI		View	Subjective
			class	instance	class	triplet		
Something-Something [26]	108K	174	-	-	174	-	first	hand
100DOH [61]	100K	11	-	110.1K	5	189.6K	first, third	hand
Something-Else [52]	8M	174	18K*	10M	174	6M	first	hand
EPIC-Kitchens [11]	266K	125	323	454K	125	243K	first	hand
CAD120++ [84]	65K	10	13	64K	2	60K	third	head, hand
VLOG [22]	114K	9	30	-	9	-	first, third	hand
AVA [27]	387K	80	-	-	51	-	third	whole body
Charades [64]	66K	157	46	41K	157	-	third	whole body
DALY [70]	11.9K	10	43	11K	10	11K	third	whole body
Action Genome [29]	234K	157	35	476K	25	1.72M	third	whole body
DIO	126K	51	1,000+	290K	51	290K	third	whole body

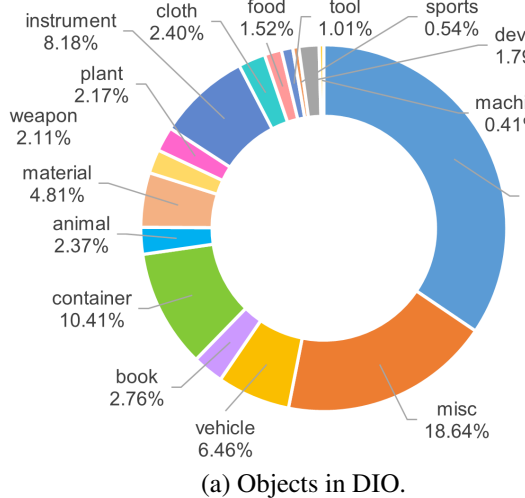
Table 1: Dataset comparison. Frames with labels are included. Instances/triplets are in *frame-level*. For clip-level annotations, we count a clip as a frame. For Action Genome [29], we count the HOIs and exclude the other relations. *18 K**: object class labels of [52] are uncurated.

clip (one interaction of a person). **First**, if there is only one object in a sub-clip, we use its locations as the labels. If there are multiple objects, we record all of their boxes and manually link their boxes as multiple object tracklets. Besides, to lower the level of discovery difficulty and simplify the evaluation, if a model can accurately discover *one* of the multiple GT objects, object discovery would be seen successfully. That said, the largest overlap between the predicted object and GT objects is calculated. **Second**, considering the costly annotation and the demand of class-agnostic object discovery, except the situation of the multi-GT object, we do not distinguish object instances in videos with *object ID* like MOT [53]. **Third**, each sub-clip is seen as a *ST-HOI tracklet*, whose label records *a human actor tracklet, an interaction, a/several class-agnostic object tracklets*.

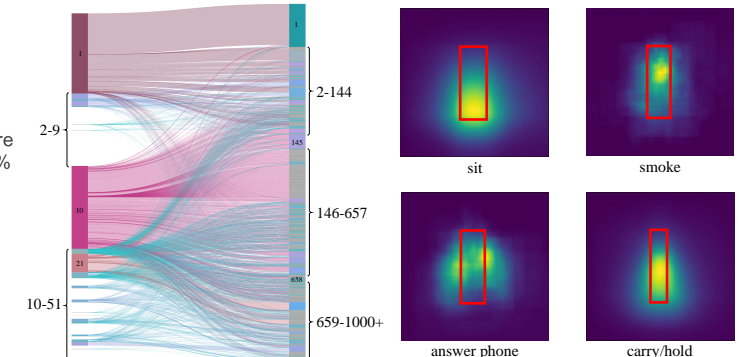
Dataset Statistics DIO includes 290 K HOI triplets, and 290 K object boxes of 1,000+ classes (Tab. 1). Compared to previous datasets, it shows an obvious demand for rare/unseen object discovery. Some characteristics are shown in Fig. 2. We split the data into train and test sets with a ratio of 5:1 (videos). For more please refer to the supplementary.

3.1. Task and Metric

Our task expects vision systems to detect ST-HOI triplets from videos. For a true positive, the **three elements** of ST-HOI, human tracking (location, id), interaction detection (location, class), and object discovery (location) all have to be accurate (Fig. 3). For human tracking, our task is similar to MOT [53] but only expects the interacting actors instead of all persons. For interaction detection, we follow the setting of AVA [27], *i.e.*, seeing it as a detection problem to detect the actors performing defined interactions. For objective discovery, since numerous classes make conventional/few/zero-shot object detectors [1, 16, 58] struggle, we set this task as class-agnostic object discovery following SOT setting [33]. Accordingly, vision systems need to first localize humans accurately as the *basis* for the subsequent two sub-tasks. Moreover, the quality of interaction detection also affects object discovery.



(a) Objects in DIO.



(b) Interaction-object co-occurrence. (c) Object location heatmap.

Figure 2: DIO characteristics. (a) Objects in DIO. (b) Co-occurrence between interactions (left) and objects (right). (c) Object location heatmaps in the train set. Red boxes indicate the normalized human location.



Figure 3: Task and metric settings. We adopt MOT [53], AVA [27], SOT [33] and a step-wise sampling strategy.

Hence, three sub-tasks are **coupled** and make the evaluation difficult. To tackle this problem, we propose an **evaluation via step-wise sampling** strategy to gradually evaluate three sub-tasks (Fig. 3). Next, we detail the metrics and evaluations of three sub-tasks.

Human Tracking. Given human tracklets, we adopt the widely-used MOTA [53] and IDF1 [59] to measure human detection and re-identification (Re-ID), which are fundamental for the subsequent two sub-tasks. Notably, a model may first track all persons and then use interaction prediction to *exclude* the persons who do not perform HOIs. A true positive actor tracklet should contain both accurate boxes (IoU>0.5 regarding GT boxes) and ID. As the annotation density of AVA is one frame per second, we evaluate two metrics according to the tracking results on the *first frame of each second* and report the mean values of all videos. According to the step-wise sampling, the **true positive** frames of actor tracking (Fig. 3, green checks) are sent to interaction detection evaluation, the rest of **false positive** frames (red crosses) are seen as false positives for two subsequent sub-tasks because the inaccuracy of actor tracking would introduce unreliable interaction and object predictions, *e.g.*, nonexistent humans or inaccurate boxes.

Interaction Detection. After measuring actor tracking, we next evaluate interaction detection, *i.e.*, which actors are

performing the defined interactions, when, and where they are performing. This is equal to instance-level action detection like AVA [27]. All predictions are in the format of ST-HOI tracklet, *i.e.*, successive frames of an actor including only one predicted continuous interaction. For all predictions, we adopt a threshold α to mask the interaction scores under α as zero. That is, if an ST-HOI tracklet for the i -th interaction a_i contains a frame with a score under α , this frame would be excluded and this tracklet would be *divided* into two ST-HOI tracklets. We adopt two metrics: **2D** and **3D IoU**. For 2D IoU, we calculate the 2D IoU between the predicted and GT boxes of each frame in an ST-HOI tracklet and get the average IoU of the whole tracklet. For 3D IoU, we link the successive human boxes as a tube and measure the 3D IoU between predicted and GT polyhedrons within one second. The mean 3D IoU of a tracklet is also calculated. A tracklet would be seen as a true positive if its mean 2D/3D IoU (mIoU) is higher than 0.2, following AVA [27]. We also set **two criteria** here. A **loose** one only measures mIoU on the true positive frames of actor tracking, thus a separate evaluation for interaction detection can be conducted. Moreover, a **strict** one considers all frames, *i.e.*, false positive frames of actor tracking (Fig. 3, red crosses) are seen as *false positives* for interaction detection too.

Interacted Object Discovery. An ST-HOI tracklet contains a/several class-agnostic GT object tracklets. For simplicity, we treat object discovery as a SOT problem and follow its metric [33]. We adopt the average overlap metric, *i.e.*, mIoU of all frames in an ST-HOI tracklet. If there are multiple GT object tracklets, we calculate all IoUs between the predicted tracklet and GT tracklets and save the largest IoU as the result. **Two criteria** are also used: (1) In the **loose** one, false positive frames from both actor tracking and interaction detection (Fig. 3, red crosses) are all discarded and not considered in the evaluation. It also provides a separate eval-

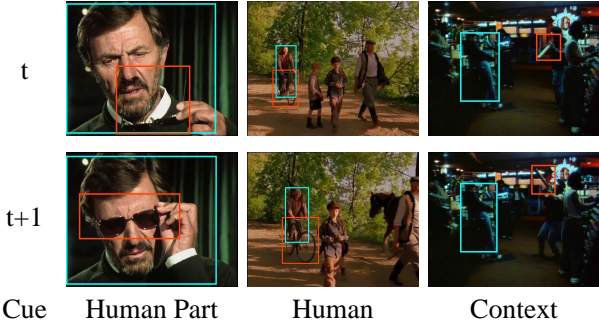


Figure 4: Three scenarios for interacted object discovery.

uation for interacted object discovery. (2) On the contrary, the **strict** one directly treats all false positive frames from the former two sub-tasks (red crosses) as *false positives* of object discovery, and their mIoUs are set to zero. The rest of the frames (green checks) are evaluated normally.

4. Method

In this section, we describe the pipeline of HPN (Fig. 5). For clarity, the description unit hereinafter is *one human tracklet* including one tracked person.

4.1. Human Tracking

Given a clip C , we first adopt FairMOT [80] or DeepSORT [71] to obtain the human tracklets: $T_h = \mathcal{F}_{track}(C)$. A human tracklet is represented as $T_h = \{I_h^k\}_{k=1}^n$ (n seconds). For T_h , we operate interaction detection next to divide it into ST-HOI tracklets including one interaction each.

4.2. Interaction Detection

Here, we adopt SlowFast [21]. As we re-split AVA, our test set contains some clips from the AVA train set, we use Kinetics [5] pre-trained backbone and finetune it on our train set to avoid *pollution*. Given a human tracklet $T_h = \{I_h^k\}_{k=1}^n$, we use 8 frames/s for slow branch and 32 frames/s for fast branch. We input slow ($[8, 2048, 7^2]$) and fast ($[32, 256, 7^2]$) RoI-Align features into the pooling layers and concatenate them as a 2,304 sized tensor, then feed it into a fully-connected (FC) layer to obtain the action score $S_a^k = \mathcal{F}_{action}(I_h^k)$, where $S_a^k = \{S_a^{ki}\}_{i=1}^{51}$, k, i indicate the indexes of second and interaction class. Interaction probabilities $p_a^k = \text{Sigmoids}(S_a^k)$. We use binary cross entropy losses for 51 interaction classes $L_a^k = (\sum_{i=1}^{51} L_a^{ki})/51$, the whole action loss of T_h is $L_a = \sum_{k=1}^n L_a^k$. The scores under threshold α will be masked to zero. If all scores of T_h are masked, we would delete T_h . Then, we divide T_h into ST-HOI tracklets including successive frames of a single interaction. As for the masking operation, one interaction may have multiple ST-HOI tracklets. For clarity, in T_h , we use T_{HOI}^i to represent the ST-HOI tracklet of a_i and omit the possible multi-tracklet.

4.3. Interacted Object Discovery

Limitations of Current Methods. It is difficult to detect objects via conventional detectors [58, 57] since the diverse/unseen objects. And zero/few-shot object detection [16, 1] also does not work well. For example, after finetuning the image-based RPN [58] and video-based detector [9] on our train set with objectiveness detection, their performances are only **12.47** and **12.25** AP. Thus, it is essential to borrow video cues to help object discovery.

Typical ST-HOI Scenarios. To get some inspiration, let us check three typical scenarios (Fig. 4). For the left $\langle human, hold, glasses \rangle$ including small glasses, we can find some cues from the moving hand, *i.e.*, *human part*. For the middle $\langle human, ride, bicycle \rangle$, as the bicycle is moving closely with the human, the *human body* can act as a cue. For the $\langle human, listen_to, instrument \rangle$, besides the human, the context (objects around human) may help us.

Hierarchical-Probe. Hence, we propose a hierarchical-probe policy to leverage three perspectives as the **starting points** of discovery. *Hierarchical* indicates that the interested region varies from **local human part** [44, 50] to **whole human**, then to **global context**. From three perspectives, we utilize visual and semantic video contents as the **conditions** to guide HPN to “search” objects. In an ST-HOI tracklet $T_{HOI}^i = \{I^k\}_{k=1}^m$ (m seconds), for its k -th second frames I^k , the visual conditions are f_h^k (human boxes) and f_c^k (whole frames), which are the features after the temporal pooling ($[2304, 7^2]$) of SlowFast; the semantic condition is f_v^i (Bert [12] vector of a_i):

$$f_h^k, f_c^k = \mathcal{F}_{slowfast}(I^k), f_v^i = \mathcal{F}_{bert}(a_i). \quad (1)$$

Next, we construct the “search” starting points as three **spatio-temporal configuration (STC)** maps (Fig. 5).

(1) For **human part**, we first use pose estimation [18, 17, 38, 37] to obtain 18 body key points. For each key-point, we prepare a $[56, 56]$ grey-scale map including a two-dimensional Gaussian distribution centering at the key-point with $\sigma_1 = \sigma_2 = 3$ pixels, to indicate part location. To distinguish the parts, we concatenate f_h^k, f_v^i and input them into an MLP-Sigmoids to generate 18 attention values a_M^k to reweight 18 keypoint maps. Then, we concatenate reweighted maps with human skeleton and box maps [45], which are all $[56, 56]$ to represent the locations of parts relative to the whole body. This $[20, 56, 56]$ tensor is used as *human part STC map* M_P^k .

(2) For **whole human body**, we use human skeleton and box maps ($[2, 56, 56]$) as the *human STC map* M_H^k .

(3) For **context**, we finetune an RPN [58] on our train set and detect the objectness in all frames. The predicted proposals after NMS are selected as the important objects in context. Thus we can construct object maps [45] with these proposals. Next, we concatenate them with human box and

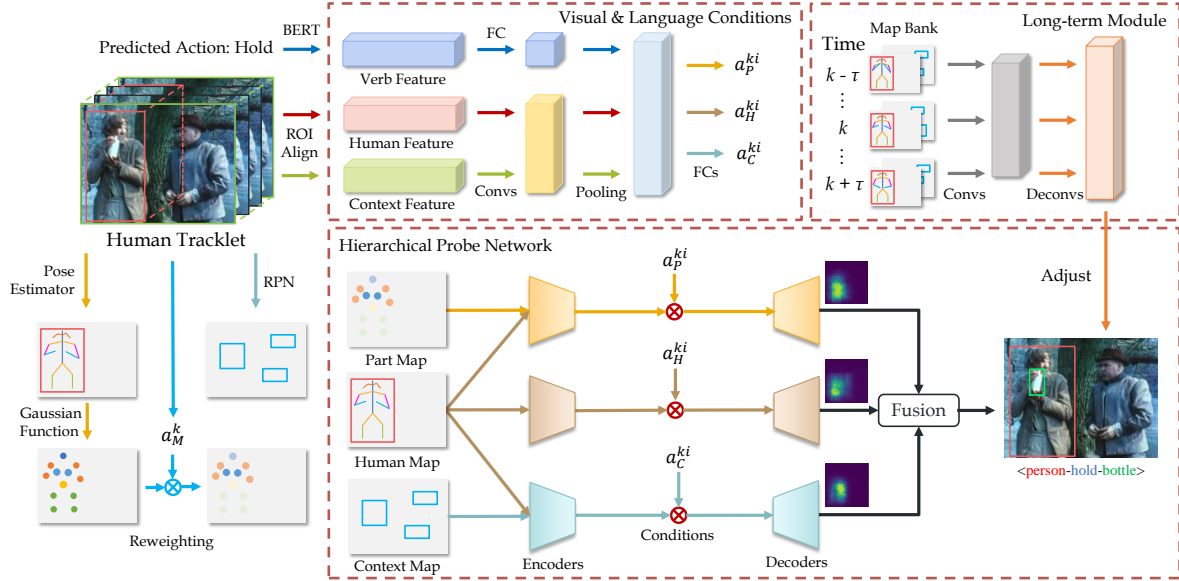


Figure 5: The overview of baseline HPN. Our hierarchical-probe policy discovers objects from 3 perspectives, *i.e.*, local human parts, human, and global context. We leverage the spatio-temporal configuration (STC) to construct three STC maps.

skeleton maps ($[2+N_p, 56, 56]$) as the *context STC map* M_C^k , where N_p is the number of proposals.

To leverage the hierarchical cues, we adopt a multi-branch structure (Fig. 5) consisting of three branches. For detailed structure please refer to our supplementary.

Part Branch. Corresponding to the *human part STC map* M_P^k , we use a convolutional encoder to embed it and obtain the compressed \hat{M}_P^k . And the condition $\langle f_h^k, f_v^i \rangle$ is also compressed into f_{hv}^{ki} . Then, we use a convolutional-Sigmoids module to transfer f_{hv}^{ki} to attention tensor a_P^{ki} which has the same channel numbers with M_P^k . The adjustment upon the part cue based on the condition is implemented as element-wise multiplication:

$$\hat{M}_P^{ki} = \hat{M}_P^k \otimes a_P^{ki}. \quad (2)$$

The superscript ki means the k -th second and a_i in an ST-HOI tracklet, and each predicted tracklet contains one person, one interaction and one class-agnostic interact object b_O^{ki} . Next, we adopt a convolutional decoder to decode \hat{M}_P^{ki} to f_P^{ki} which is the same size as video frames. At last, we use pixel-level Sigmoids to translate f_P^{ki} into a heatmap which can illustrate the object location: $h_P^{ki} = \text{Sigmoids}(f_P^{ki})$. For each GT object box, a chosen GT heatmap h_{GT}^{ki} is constructed by generating a 2-dimensional Gaussian distribution centering at the GT box center with σ_1, σ_2 as half of the box width and height. The pixel-wise Sigmoid cross entropy (BCE) loss L_P^{ki} is employed for h_P^{ki} .

Human and Context Branches. Their structures are similar to the part branch. First, we compress M_H^k, M_C^k into \hat{M}_H^k, \hat{M}_C^k with two convolutional encoders. Then the conditions $\langle f_h^k, f_v^i \rangle$ for human branch and $\langle f_h^k, f_c^k, f_v^i \rangle$ for context branch are compressed into f_{hv}^{ki} and f_{hcv}^{ki} respectively.

We use two convolutional-Sigmoids modules to transfer f_{hv}^{ki} to a_P^{ki}, a_H^{ki} , and f_{hcv}^{ki} to a_C^{ki} . The adjustments are similar:

$$\begin{aligned} \hat{M}_H^{ki} &= \hat{M}_H^k \otimes a_H^{ki}, \\ \hat{M}_C^{ki} &= \hat{M}_C^k \otimes a_C^{ki}. \end{aligned} \quad (3)$$

Two decoders are then used to decode $\hat{M}_H^{ki}, \hat{M}_C^{ki}$ to f_H^{ki}, f_C^{ki} . The two output heatmaps are obtained via $h_H^{ki} = \text{Sigmoids}(f_H^{ki}), h_C^{ki} = \text{Sigmoids}(f_C^{ki})$. And the corresponding pixel-wise BCE losses are L_H^{ki}, L_C^{ki} .

Object Size Classification. As objects with different sizes have different localization difficulties, *e.g.*, small objects are usually harder to discover (proven in Sec. 5). To enable HPN to distinguish object size and take corresponding heatmap filtering strategies, we further adopt a simple object size classifier. First, for objects in train and val sets, we calculate the areas of GT human a_h and object a_o and calculate the ratio between them: $r_{o|h} = a_o/a_h$. Then, $r_{o|h}$ is used to separate the GT objects into three size classes: small ($r_{o|h} \leq 0.3$), medium ($0.3 < r_{o|h} \leq 1$), large ($r_{o|h} > 1$). Finally, we introduce a two-layer MLP classifier with Softmax, its input is the concatenation of f_c^k and f_h^k . For the object of the k -th second and i -th interaction, it would predict its size class. A cross-entropy loss L_{size}^{ki} is used to train it. In testing, the classified size would decide the heatmap filtering threshold (Sec. 5.3).

Perspective Fusion. For heatmaps $h_{P/H/C}^{ki}$, after normalizing and filtering with a threshold, we can generate the tightest bounding boxes for the binary masks as the predicted locations. As the three branches are complementary, we fuse their predictions with three strategies: **(1) Equal Fusion:** directly fusing $h_P^{ki}, h_H^{ki}, h_C^{ki}$ with $h^{ki} = 1/3(h_P^{ki} +$

$h_H^{ki} + h_C^{ki}$) to get box b_O^{ki} . **(2) Box Selection:** obtaining boxes from heatmaps, *i.e.*, $b_{PO}^{ki}, b_{HO}^{ki}, b_{CO}^{ki}$, and building a val set by randomly choosing 50 videos from train set to evaluate them. For a_i , we select a branch prediction that performed best on val set. **(3) Dynamic Fusion:** concatenating $\hat{M}_P^k, \hat{M}_H^k, \hat{M}_C^k$ and inputting them into an FC-Softmax to generate dynamic fusion factors $\beta_P, \beta_H, \beta_C$, then $h^{ki} = \beta_P h_P^{ki} + \beta_H h_H^{ki} + \beta_C h_C^{ki}$. On val set, dynamic fusion performs best and is chosen as our final setting.

Long-Term Information. Besides the short-term cues of one second utilized above, long-term cues are also proven effective in video understanding [72]. Thus, we adopt a module to capture long-term cues and generate a heatmap to complement the short-term prediction. For the k -th second, we construct a *STC map flow* belonging to time range $[k - \tau, k + \tau]$ by concatenating the STC (skeleton, human box, proposals) maps of $[k - \tau, k + \tau]$, where τ is the time offset and set as 2 in practice. Insufficient seconds will be filled with empty maps as placeholders. For the STC flow ($[N, 2 + N_p, 2\tau + 1, 56, 56]$), we use three 3D convolution layers to aggregate the local ST information, a non-local layer to pass the information between local ST ranges, a temporal pooling layer to associate in the time dimension, and five 2D deconvolution layers to generate the heatmap. The heatmaps from short-term and long-term modules are fused with weights ϵ and $1 - \epsilon$. Finally, we operate filtering upon the fused heatmap to obtain the final predicted object box.

Losses. The object discovery loss for $T_{HOI}^i = \{I^k\}_{k=1}^m$ is $L_o^i = \sum_{k=1}^m (L_P^{ki} + L_H^{ki} + L_C^{ki} + L_{size}^{ki})$. For a human tracklet T_h , the object discovery loss is $L_o = (\sum_{i=1}^{51} L_o^i)/51$. The total loss of T_h is $L = L_a + L_o$ (L_a in Sec. 4.2).

5. Experiments

5.1. Settings

We report the results following Sec. 3.1. For human tracking, we calculate the MOTA [53] and IDF1 [59]. After step-wise sampling, the 2D/3D mIoU under strict/loose criteria is reported for action detection and object discovery.

5.2. Baselines

To tackle challenging interacted object discovery, we look back to previous methods, analyze their characteristics and propose several baselines. We present the baselines in descending order of the reliance on object detection. As our main goal is to explore the interacted object discovery, for a fair comparison, all baselines adopt the same human trackers, interaction classifier, and backbone with HPN. More details are described in the supplementary.

Proposal-based Baselines: With the RPN [58] finetuned on the train set, we obtain the proposals of each frame in an ST-HOI tracklet. Here, four proposal-based base-

lines are adopted: (1) **Proposal Selection (PS)** [65] selects the proposal generating the highest interaction classification score. (2) **Proposal+Tracking-By-Detection (PTBD)** uses TBD [78] to match proposals into tracklets and chooses the one generating the highest mean interaction score. (3) **Proposal+Single Object Tracking (PSOT)** tracks each proposal via SOT [36] and chooses the one generating the highest mean interaction score. (4) **Proposal Adjustment (PA)** [8] chooses a proposal with the highest objectness confidence and learns the offset between it and the GT box.

Human-to-Object (HTO) [25] directly adjusts the human box to the object box via a learned offset.

Density Estimation (DE) [25] sees object discovery as density estimation to estimate the object location likelihood and multiplies this likelihood with the interaction score.

Shortest Distance (SD) [61] learns an offset from human to object similar to HTO and chooses a proposal having the shortest center distance with the HTO estimated box.

Heatmap (HM) [32] directly inputs the *condition* feature, skeleton map, and verb vector to estimate the heatmap.

Box Regression (BR) directly regresses the object box.

5.3. Implementation Details

Human Tracking. FairMOT [80] and DeepSORT [71] are adopted and frozen. For DeepSORT, we use the open-sourced version with YOLO [57] and pre-trained weights. For FairMOT, its pre-trained detector performs unsatisfied because of the domain gap between pedestrian data and AVA [27]. So we adopt YOLO [57] as its detector and only use its feature extractor pre-trained on multi-dataset [63, 13, 79, 74, 81, 14, 53].

Interaction Detection. SlowFast [21] model pre-trained on Kinetics-700 [5] from [66] is finetuned on our train set for 24 epochs. We use an SGD optimizer, an initial learning rate of 4e-3, cosine learning rate decay, and a batch size of 16. A simple FC-Sigmoid classifier is used to classify interactions. In training, we finetune the object discovery modules HPN-C, HPN-H, and HPN-P for 7, 22, and 11 epochs respectively.

Object Discovery. To prepare the proposals, we finetune a COCO [46] pre-trained RPN on the train set with GT boxes for 35K iterations. An SGD optimizer, a learning rate of 8e-4, and a batch size of 24 are adopted. We jointly train the object module and interaction classifier together for 1 epoch for HPN. For DE with DeepSORT and FairMOT, we set the threshold α as 0.2 and 0.5. For proposal-based methods with DeepSORT, α is set as 0.02. For the other methods, α is set as 0.03 and 0.4 for DeepSORT and FairMOT. For baselines, we use the same learning rate and batch size as interaction detection. For single branch HPN-P/H/C, the heatmap filtering thresholds are all 0.6. For HPN, the thresholds for small, medium, and large objects are 0.7, 0.6, and 0.5 respectively. In the long-term module, ϵ is 0.1. The

Human Tracking	Methods	Human Tracking		Interaction Detection (mAP(%))				Object Discovery (mIoU(%))			
		MOTA(%)	IDF1(%)	Strict		Loose		Strict		Loose	
				2D	3D	2D	3D	2D	3D	2D	3D
DeepSORT	Proposal Selection (PS)	15.9	44.1	9.5	5.5	10.2	6.0	1.1	0.9	14.0	17.3
	Proposal + TBD (PTBD)	15.9	44.1	9.5	5.4	10.2	6.0	1.1	0.9	14.6	18.0
	Proposal + SOT (PSOT)	15.9	44.1	9.3	5.4	10.1	6.2	1.1	0.9	13.9	17.1
	Proposal Adjustment (PA)	15.9	44.1	9.3	5.4	10.0	6.0	1.3	1.0	16.7	20.5
	Human-to-Object (HTO)	15.9	44.1	8.9	5.6	9.3	6.3	1.5	1.2	19.2	23.7
	Density Estimation (DE)	20.0	44.6	11.9	6.8	12.3	7.5	2.5	2.1	22.1	26.4
	Shortest Distance (SD)	15.9	44.1	9.4	5.4	10.1	5.9	1.4	1.1	18.0	22.3
	HeatMap (HM)	15.9	44.1	8.3	5.1	9.0	5.5	1.4	1.1	18.3	22.6
	Box Regression (BR)	15.9	44.1	8.7	5.4	9.3	5.8	0.9	0.7	12.2	14.9
	HPN-P	15.9	44.1	8.4	4.7	8.8	5.2	1.4	1.1	20.6	25.4
	HPN-H	15.9	44.1	8.2	4.7	8.6	5.2	1.4	1.1	19.7	24.2
	HPN-C	15.9	44.1	9.0	5.2	9.5	5.8	1.6	1.3	22.2	27.8
FairMOT	HPN	17.3	44.2	9.7	5.4	10.0	6.1	1.6	1.3	24.6	30.4
	Proposal Selection (PS)	3.9	45.5	3.6	2.1	3.8	2.6	2.5	2.0	15.1	18.5
	Proposal + TBD (PTBD)	3.9	45.5	3.6	2.1	3.7	2.6	2.6	2.1	15.6	19.1
	Proposal + SOT (PSOT)	3.9	45.5	3.6	2.1	3.8	2.5	2.5	2.0	15.2	18.7
	Proposal Adjustment (PA)	4.4	46.0	3.8	2.2	4.1	2.6	2.7	2.2	17.9	22.1
	Human-to-Object (HTO)	3.8	45.7	4.4	2.4	4.5	2.7	3.0	2.4	19.1	23.4
	Density Estimation (DE)	20.2	45.9	4.3	2.4	4.4	2.7	6.6	5.4	25.2	30.2
	Shortest Distance (SD)	3.9	45.5	3.5	2.1	3.7	2.5	3.3	2.6	19.6	23.9
	HeatMap (HM)	4.3	45.9	4.4	2.4	4.6	2.6	2.8	2.2	18.6	22.9
	Box Regression (BR)	4.3	45.9	4.2	2.4	4.3	2.7	2.0	1.6	13.1	16.0
	HPN-P	5.0	45.7	4.3	2.6	4.5	2.8	3.2	2.5	21.5	26.5
	HPN-H	5.0	45.7	4.3	2.7	4.5	3.0	3.0	2.4	20.5	25.3
	HPN-C	4.6	45.9	4.4	2.4	4.6	2.8	3.7	2.9	24.2	29.7
	HPN	11.1	47.0	5.0	2.9	5.2	3.4	4.0	3.2	26.4	32.0

Table 2: Results on DIO. HPN-P/H/C indicates the single branch in HPN without dynamic fusion.

number of proposals N_p in HPN-C is 75. These thresholds are obtained by grid search on val set.

5.4. Results

We report the results of HPN and baselines in Tab. 2.

Human Tracking. For MOTA, DeepSORT largely surpasses FairMOT due to its person ID stability. Since we only evaluate the individual seconds, the gap is more obvious. However, the IDF1 of FairMOT is slightly higher, which means the overall Re-ID accuracy of FairMOT is better. Compared to FairMOT, the performances of baselines with DeepSORT is more robust, due to the strong tracking stability of DeepSORT. Surprisingly, DE achieves impressive performance. Probably because it uses the proposal location probability to adjust the interaction score (Sec. 5.2), which can suppress the human-object pairs with low correlations and decrease the low-grade tracklets. Relatively, HPN also shows decent improvements upon the other baselines and outperforms all methods on IDF1 of FairMOT.

Interaction Detection. Since we use the same Slowfast backbone and human tracking inputs, the performance variance of all methods is marginal. Given FairMOT, HPN outperforms all baselines with the help of object and interaction joint training. Meanwhile, with DeepSORT, DE achieves decent performance as it also considers two entangled tasks together. But it performs worse than HPN with FairMOT, possibly because the person ID is unstable.

Object Discovery. HPN effectively captures the essential video cues and achieves great improvements under loose criterion, *e.g.*, 2.5% and 4.0% improvements upon DE (DeepSORT). But under strict criterion considering the

quality of human tracking and interaction detection, DE is better. Meanwhile, HTO also shows superiority over the other baselines. These indicate that heatmap/proposal-based methods are promising for object discovery. But regression-based methods may lack the ability to locate these objects. If only keeping one branch in HPN (HPN-P/H/C in Tab. 2), the context branch performs best. And they show obvious complementary properties, thus resulting in great improvement after the dynamic fusion. Moreover, all methods perform unsatisfied under strict criterion because of the poor performances of human tracking and interaction detection. Hence, DIO poses a great challenge to vision systems and requires more studies on three sub-tasks.

Visualizations. In Fig. 6, we analyze the object discovery results in different views, such as rare/unrare/unseen objects, size, *etc.*, where HPN shows superiority.

5.5. Ablation Study

We randomly choose 50 videos from the train set as val set for the ablation study on interacted object discovery. HPN-C is chosen as the baseline, which achieves the best **32.2** mIoU (loose 3D) in the default setting, except for dynamic fusion. Detailed table please refer to our supplementary.

(1) Losses: replacing the BCE loss for regression with L1, L2 losses causes obvious degradations (**26.3**, **29.2** mIoU).

(2) Fusion: in three policies, dynamic fusion gets the best **35.9** mIoU, whilst equal fusion and prediction selection get **32.9** and **35.2** mIoU.

(3) Condition: in default, we translate the conditions

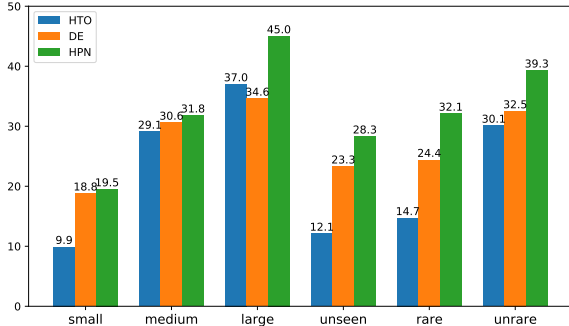


Figure 6: Object discovery analysis (DeepSORT, loose 3D).

into attentions, here we directly concatenate the conditioned feature with the perspective feature but perform worse (**31.1** mIoU).

(4) Proposal: we change the proposal numbers to 50 and 100 (**32.1**, **32.1** mIoU) in the context STC map, but are all worse than 75. **(5) Long-term Range:** we extend the long-term offset to 3 and 4 (**26.1**, **26.3** mIoU), but they are all worse than 2 (**27.9** mIoU).

6. Conclusion

In this work, we propose a novel ST-HOI learning task and construct a corresponding benchmark DIO. It contains 1,000+ object classes in 290K frame-level HOI triplets. To tackle this challenging task, we propose a hierarchical-probe network (HPN) and achieve decent results. However, DIO remains challenging, even after adopting state-of-the-art tools and methods. We believe it would inspire a new line of research on deeper activity understanding.

References

- [1] Ankan Bansal, Karan Sikka, Gaurav Sharma, Rama Chellappa, and Ajay Divakaran. Zero-shot object detection. In *ECCV*, 2018. [2](#), [3](#), [5](#)
- [2] Fabien Baradel, Natalia Neverova, Christian Wolf, Julien Mille, and Greg Mori. Object level visual reasoning in videos. In *ECCV*, 2018. [2](#)
- [3] Guillem Brasó and Laura Leal-Taixé. Learning a neural solver for multiple object tracking. In *CVPR*, 2020. [2](#), [17](#)
- [4] Fabian Caba Heilbron, Victor Escorcia, Bernard Ghanem, and Juan Carlos Niebles. Activitynet: A large-scale video benchmark for human activity understanding. In *CVPR*, 2015. [2](#)
- [5] Joao Carreira, Eric Noland, Chloe Hillier, and Andrew Zisserman. A short note on the kinetics-700 human action dataset. *arXiv preprint arXiv:1907.06987*, 2019. [5](#), [7](#)
- [6] Yu-Wei Chao, Yunfan Liu, Xieyang Liu, Huayi Zeng, and Jia Deng. Learning to detect human-object interactions. In *WACV*, 2018. [1](#), [2](#)
- [7] Yu Wei Chao, Zhan Wang, Yugeng He, Jiaxuan Wang, and Jia Deng. Hico: A benchmark for recognizing human-object interactions in images. In *ICCV*, 2015. [2](#)
- [8] Guobin Chen, Wongun Choi, Xiang Yu, Tony Han, and Manmohan Chandraker. Learning efficient object detection models with knowledge distillation. In *NIPS*, pages 742–751, 2017. [7](#), [17](#)
- [9] Yihong Chen, Yue Cao, Han Hu, and Liwei Wang. Memory enhanced global-local aggregation for video object detection. In *CVPR*, 2020. [2](#), [3](#), [5](#)
- [10] Zedu Chen, Bineng Zhong, Guorong Li, Shengping Zhang, and Rongrong Ji. Siamese box adaptive network for visual tracking. In *CVPR*, 2020. [2](#)
- [11] Dima Damen, Hazel Doughty, Giovanni Maria Farinella, Sanja Fidler, Antonino Furnari, Evangelos Kazakos, Davide Moltisanti, Jonathon Munro, Toby Perrett, Will Price, et al. Scaling egocentric vision: The epic-kitchens dataset. In *ECCV*, 2018. [1](#), [2](#), [3](#), [12](#), [14](#)
- [12] Jacob Devlin, Ming-Wei Chang, Kenton Lee, and Kristina Toutanova. Bert: Pre-training of deep bidirectional transformers for language understanding. *arXiv preprint arXiv:1810.04805*, 2018. [5](#)
- [13] Piotr Dollár, Christian Wojek, Bernt Schiele, and Pietro Perona. Pedestrian detection: A benchmark. In *CVPR*, 2009. [7](#)
- [14] Andreas Ess, Bastian Leibe, Konrad Schindler, and Luc Van Gool. A mobile vision system for robust multi-person tracking. In *CVPR*, 2008. [7](#)
- [15] Heng Fan, Liting Lin, Fan Yang, Peng Chu, Ge Deng, Sijia Yu, Hexin Bai, Yong Xu, Chunyuan Liao, and Haibin Ling. Lasot: A high-quality benchmark for large-scale single object tracking. In *CVPR*, 2019. [2](#)
- [16] Qi Fan, Wei Zhuo, Chi-Keung Tang, and Yu-Wing Tai. Few-shot object detection with attention-rpn and multi-relation detector. In *CVPR*, 2020. [2](#), [3](#), [5](#)
- [17] Hao-Shu Fang, Jiefeng Li, Hongyang Tang, Chao Xu, Haoyi Zhu, Yuliang Xiu, Yong-Lu Li, and Cewu Lu. Alpha-pose: Whole-body regional multi-person pose estimation and tracking in real-time. *IEEE Transactions on Pattern Analysis and Machine Intelligence*, 2022. [5](#)
- [18] Hao-Shu Fang, Shuqin Xie, Yu-Wing Tai, and Cewu Lu. Rmpe: Regional multi-person pose estimation. In *ICCV*, 2017. [5](#)
- [19] Hao-Shu Fang, Yichen Xie, Dian Shao, Yong-Lu Li, and Cewu Lu. Decaug: Augmenting hoi detection via decomposition. In *AAAI*, 2021. [1](#)
- [20] Hao-Shu Fang, Yichen Xie, Dian Shao, and Cewu Lu. Dirv: Dense interaction region voting for end-to-end human-object interaction detection. In *AAAI*, 2021. [2](#)
- [21] Christoph Feichtenhofer, Haoqi Fan, Jitendra Malik, and Kaiming He. Slowfast networks for video recognition. In *ICCV*, 2019. [5](#), [7](#)
- [22] David F Fouhey, Wei-cheng Kuo, Alexei A Efros, and Jitendra Malik. From lifestyle vlogs to everyday interactions. In *CVPR*, 2018. [2](#), [3](#)
- [23] Chen Gao, Yuliang Zou, and Jia-Bin Huang. ican: Instance-centric attention network for human-object interaction detection. *arXiv preprint arXiv:1808.10437*, 2018. [1](#), [2](#)
- [24] Rohit Girdhar, Joao Carreira, Carl Doersch, and Andrew Zisserman. Video action transformer network. In *CVPR*, 2019. [2](#)

[25] Georgia Gkioxari, Ross Girshick, Piotr Dollár, and Kaiming He. Detecting and recognizing human-object interactions. In *CVPR*, 2018. 2, 7, 17

[26] Raghav Goyal, Samira Ebrahimi Kahou, Vincent Michalski, Joanna Materzynska, Susanne Westphal, Heuna Kim, Valentin Haenel, Ingo Fruend, Peter Yianilos, Moritz Mueller-Freitag, et al. The “something something” video database for learning and evaluating visual common sense. In *ICCV*, 2017. 3

[27] Chunhui Gu, Chen Sun, David A Ross, Carl Vondrick, Caroline Pantofaru, Yeqing Li, Sudheendra Vijayanarasimhan, George Toderici, Susanna Ricco, Rahul Sukthankar, Cordelia Schmid, and Jitendra Malik. Ava: A video dataset of spatio-temporally localized atomic visual actions. In *CVPR*, 2018. 1, 2, 3, 4, 7, 12

[28] Han Hu, Jiayuan Gu, Zheng Zhang, Jifeng Dai, and Yichen Wei. Relation networks for object detection. In *CVPR*, 2018. 2

[29] Jingwei Ji, Ranjay Krishna, Li Fei-Fei, and Juan Carlos Niebles. Action genome: Actions as compositions of spatio-temporal scene graphs. In *CVPR*, 2020. 1, 2, 3, 14

[30] Keizo Kato, Yin Li, and Abhinav Gupta. Compositional learning for human object interaction. In *ECCV*, 2018. 1, 2

[31] Chanho Kim, Fuxin Li, Arridhana Ciptadi, and James M Rehg. Multiple hypothesis tracking revisited. In *ICCV*, 2015. 2

[32] Daesik Kim, Gyujeong Lee, Jisoo Jeong, and Nojun Kwak. Tell me what they’re holding: Weakly-supervised object detection with transferable knowledge from human-object interaction. In *AAAI*, 2020. 2, 7, 17

[33] Matej Kristan, Ales Leonardis, Jiri Matas, Michael Felsberg, Roman Pflugfelder, Luka Cehovin Zajc, Tomas Vojir, Goutam Bhat, Alan Lukezic, Abdelrahman Elde索key, et al. The sixth visual object tracking vot2018 challenge results. In *ECCV*, 2018. 3, 4

[34] Ivan Laptev and Patrick Pérez. Retrieving actions in movies. In *ICCV*, 2007. 1

[35] Hei Law and Jia Deng. Cornernet: Detecting objects as paired keypoints. In *Proceedings of the European Conference on Computer Vision (ECCV)*, pages 734–750, 2018. 17

[36] Bo Li, Junjie Yan, Wei Wu, Zheng Zhu, and Xiaolin Hu. High performance visual tracking with siamese region proposal network. In *CVPR*, pages 8971–8980, 2018. 7, 17

[37] Jiefeng Li, Siyuan Bian, Ailing Zeng, Can Wang, Bo Pang, Wentao Liu, and Cewu Lu. Human pose regression with residual log-likelihood estimation. In *ICCV*, 2021. 5

[38] Jiefeng Li, Can Wang, Hao Zhu, Yihuan Mao, Hao-Shu Fang, and Cewu Lu. Crowdpose: Efficient crowded scenes pose estimation and a new benchmark. In *CVPR*, 2019. 5

[39] Yong-Lu Li, Xinpeng Liu, Han Lu, Shiyi Wang, Junqi Liu, Jiefeng Li, and Cewu Lu. Detailed 2d-3d joint representation for human-object interaction. In *CVPR*, 2020. 2

[40] Yong-Lu Li, Xinpeng Liu, Xiaoqian Wu, Xijie Huang, Liang Xu, and Cewu Lu. Transferable interactiveness knowledge for human-object interaction detection. In *TPAMI*, 2022. 2

[41] Yong-Lu Li, Xinpeng Liu, Xiaoqian Wu, Yizhuo Li, and Cewu Lu. Hoi analysis: Integrating and decomposing human-object interaction. In *NeurIPS*, 2020. 1, 2

[42] Yong-Lu Li, Xinpeng Liu, Xiaoqian Wu, Yizhuo Li, Zuoyu Qiu, Liang Xu, Yue Xu, Hao-Shu Fang, and Cewu Lu. Hake: A knowledge engine foundation for human activity understanding. *arXiv preprint arXiv:2202.06851*, 2022. 2

[43] Yong-Lu Li, Liang Xu, Xinpeng Liu, Xijie Huang, Yue Xu, Mingyang Chen, Ze Ma, Shiyi Wang, Hao-Shu Fang, and Cewu Lu. Hake: Human activity knowledge engine. *arXiv preprint arXiv:1904.06539*, 2019. 2

[44] Yong-Lu Li, Liang Xu, Xinpeng Liu, Xijie Huang, Yue Xu, Shiyi Wang, Hao-Shu Fang, Ze Ma, Mingyang Chen, and Cewu Lu. Pastanet: Toward human activity knowledge engine. In *CVPR*, 2020. 1, 2, 5

[45] Yong-Lu Li, Siyuan Zhou, Xijie Huang, Liang Xu, Ze Ma, Hao-Shu Fang, Yanfeng Wang, and Cewu Lu. Transferable interactiveness knowledge for human-object interaction detection. In *CVPR*, 2019. 2, 5

[46] Tsung Yi Lin, Michael Maire, Serge Belongie, James Hays, Pietro Perona, Deva Ramanan, Piotr Dollár, and C. Lawrence Zitnick. Microsoft coco: Common objects in context. In *ECCV*, 2014. 2, 3, 7

[47] Chenchen Liu, Yang Jin, Kehan Xu, Guoqiang Gong, and Yadong Mu. Beyond short-term snippet: Video relation detection with spatio-temporal global context. In *CVPR*, 2020. 2

[48] Xinpeng Liu, Yong-Lu Li, and Cewu Lu. Highlighting object category immunity for the generalization of human-object interaction detection. In *AAAI 2022*, 2022. 2

[49] Xinpeng Liu, Yong-Lu Li, Xiaoqian Wu, Yu-Wing Tai, Cewu Lu, and Chi-Keung Tang. Interactiveness field in human-object interactions. In *CVPR*, 2022. 1

[50] Cewu Lu, Hao Su, Yong-Lu Li, Yongyi Lu, Li Yi, Chi-Keung Tang, and Leonidas J Guibas. Beyond holistic object recognition: Enriching image understanding with part states. In *CVPR*, 2018. 5

[51] Chih-Yao Ma, Asim Kadav, Iain Melvin, Zsolt Kira, Ghassan AlRegib, and Hans Peter Graf. Attend and interact: Higher-order object interactions for video understanding. In *CVPR*, 2018. 2

[52] Joanna Materzynska, Tete Xiao, Roei Herzig, Huijuan Xu, Xiaolong Wang, and Trevor Darrell. Something-else: Compositional action recognition with spatial-temporal interaction networks. In *CVPR*, 2020. 1, 2, 3

[53] Anton Milan, Laura Leal-Taixé, Ian Reid, Stefan Roth, and Konrad Schindler. Mot16: A benchmark for multi-object tracking. *arXiv preprint arXiv:1603.00831*, 2016. 2, 3, 4, 7, 17

[54] George A Miller. Wordnet: a lexical database for english. *Communications of the ACM*, 1995. 3, 12

[55] Alessandro Prest, Vittorio Ferrari, and Cordelia Schmid. Explicit modeling of human-object interactions in realistic videos. *TPAMI*, 2012. 1

[56] Siyuan Qi, Wenguan Wang, Baoxiong Jia, Jianbing Shen, and Song-Chun Zhu. Learning human-object interactions by graph parsing neural networks. In *ECCV*, 2018. 1, 2

[57] Joseph Redmon, Santosh Divvala, Ross Girshick, and Ali Farhadi. You only look once: Unified, real-time object detection. In *CVPR*, 2016. 2, 3, 5, 7

[58] Shaoqing Ren, Kaiming He, Ross Girshick, and Jian Sun. Faster r-cnn: Towards real-time object detection with region proposal networks. In *NIPS*, 2015. 2, 3, 5, 7, 16

[59] Ergys Ristani, Francesco Solera, Roger Zou, Rita Cucchiara, and Carlo Tomasi. Performance measures and a data set for multi-target, multi-camera tracking. In *ECCV*, 2016. 2, 4, 7, 17

[60] Amir Sadeghian, Alexandre Alahi, and Silvio Savarese. Tracking the untrackable: Learning to track multiple cues with long-term dependencies. In *CVPR*, 2017. 2

[61] Dandan Shan, Jiaqi Geng, Michelle Shu, and David F Fouhey. Understanding human hands in contact at internet scale. In *CVPR*, 2020. 1, 2, 3, 7

[62] Xindi Shang, Tongwei Ren, Jingfan Guo, Hanwang Zhang, and Tat-Seng Chua. Video visual relation detection. In *ACMMM*, 2017. 2

[63] Shuai Shao, Zijian Zhao, Boxun Li, Tete Xiao, Gang Yu, Xiangyu Zhang, and Jian Sun. Crowdhuman: A benchmark for detecting human in a crowd. *arXiv preprint arXiv:1805.00123*, 2018. 7

[64] Gunnar A Sigurdsson, GÜl Varol, Xiaolong Wang, Ali Farhadi, Ivan Laptev, and Abhinav Gupta. Hollywood in homes: Crowdsourcing data collection for activity understanding. In *ECCV*, 2016. 1, 2, 3

[65] Zhiyu Tan, Xuecheng Nie, Qi Qian, Nan Li, and Hao Li. Learning to rank proposals for object detection. In *ICCV*, 2019. 7, 16

[66] Jiajun Tang, Jin Xia, Xinzheng Mu, Bo Pang, and Cewu Lu. Asynchronous interaction aggregation for action detection. In *ECCV*, 2020. 7

[67] Zhi Tian, Chunhua Shen, Hao Chen, and Tong He. Fcos: Fully convolutional one-stage object detection. In *Proceedings of the IEEE international conference on computer vision*, pages 9627–9636, 2019. 17

[68] Yao-Hung Hubert Tsai, Santosh Divvala, Louis-Philippe Morency, Ruslan Salakhutdinov, and Ali Farhadi. Video relationship reasoning using gated spatio-temporal energy graph. In *CVPR*, 2019. 2

[69] Xiaolong Wang and Abhinav Gupta. Videos as space-time region graphs. In *ECCV*, 2018. 2

[70] Philippe Weinzaepfel, Xavier Martin, and Cordelia Schmid. Human action localization with sparse spatial supervision. *arXiv preprint arXiv:1605.05197*, 2016. 1, 2, 3

[71] Nicolai Wojke, Alex Bewley, and Dietrich Paulus. Simple online and realtime tracking with a deep association metric. In *ICIP*, 2017. 2, 5, 7, 17

[72] Chao-Yuan Wu, Christoph Feichtenhofer, Haoqi Fan, Kaiming He, Philipp Krahenbuhl, and Ross Girshick. Long-term feature banks for detailed video understanding. In *CVPR*, 2019. 7

[73] Xiaoqian Wu, Yong-Lu Li, Xinpeng Liu, Junyi Zhang, Yuzhe Wu, and Cewu Lu. Mining cross-person cues for body-part interactiveness learning in hoi detection. In *ECCV*, 2022. 1

[74] Tong Xiao, Shuang Li, Bochao Wang, Liang Lin, and Xiaogang Wang. End-to-end deep learning for person search. *arXiv preprint arXiv:1604.01850*, 2(2), 2016. 7

[75] Xinyu Xu, Yong-Lu Li, and Cewu Lu. Learning to anticipate future with dynamic context removal. In *CVPR*, 2022. 2

[76] Zhenheng Yang, Dhruv Mahajan, Deepti Ghadiyaram, Ram Nevatia, and Vignesh Ramanathan. Activity driven weakly supervised object detection. In *CVPR*, 2019. 2, 17

[77] Yuan Yuan, Xiaodan Liang, Xiaolong Wang, Dit-Yan Yeung, and Abhinav Gupta. Temporal dynamic graph lstm for action-driven video object detection. In *ICCV*, 2017. 2

[78] Li Zhang, Yuan Li, and Ramakant Nevatia. Global data association for multi-object tracking using network flows. In *CVPR*, 2008. 7, 17

[79] Shanshan Zhang, Rodrigo Benenson, and Bernt Schiele. Citypersons: A diverse dataset for pedestrian detection. In *CVPR*, 2017. 7

[80] Yifu Zhang, Chunyu Wang, Xinggang Wang, Wenjun Zeng, and Wenyu Liu. Fairmot: On the fairness of detection and re-identification in multiple object tracking. In *arxiv*, 2020. 2, 5, 7, 17

[81] Liang Zheng, Hengheng Zhang, Shaoyan Sun, Manmohan Chandraker, Yi Yang, and Qi Tian. Person re-identification in the wild. In *CVPR*, 2017. 7

[82] Bolei Zhou, Alex Andonian, Aude Oliva, and Antonio Torralba. Temporal relational reasoning in videos. In *ECCV*, 2018. 1, 2

[83] Xingyi Zhou, Dequan Wang, and Philipp Krähenbühl. Objects as points. *arXiv preprint arXiv:1904.07850*, 2019. 17

[84] Tao Zhuo, Zhiyong Cheng, Peng Zhang, Yongkang Wong, and Mohan Kankanhalli. Explainable video action reasoning via prior knowledge and state transitions. In *ACMMM*, 2019. 1, 3

The contents of this supplementary material are:

Sec. A: Characteristics of DIO.

Sec. B: Detailed model structure.

Sec. C: Detailed implementation of the baselines.

Sec. D: Detailed ablation study.

Sec. E: Visualized results of object discovery.

Sec. F: Testing results with GT as inputs.

A. More characteristics of DIO

A.1. Video Selection for DIO Test Set

To make DIO challenging and practical, we construct its test set via seeing video selection as a **multi-objective integer programming** problem.

First, given the video number N , interaction class number N_a , object class number N_o and GT object location heatmap size N_h (the original size of AVA [27] frames is resized to the size of the heatmap, and here we use a 1D vector to represent the values of original 2D heatmap) in AVA train-val sets, we define a binary variable $x_i \in \{0, 1\}$, $1 \leq i \leq N$ for each video to indicate whether to choose it or not for our test set. We restrict the sum of x_i to the number of videos in the test set (N_t) according to a certain split ratio.

Second, for video i , we calculate its distributions of interaction class $\mathbf{a}_i \in \mathbb{N}^{N_a}$ (a set of interaction class frequencies), object class $\mathbf{o}_i \in \mathbb{N}^{N_o}$ (a set of object class frequencies), and object location GT heatmap $\mathbf{c}_i \in \mathbb{N}^{N_h}$. Each x_i is multiplied to \mathbf{a}_i , \mathbf{o}_i and \mathbf{c}_i individually, then we add them up respectively to obtain three total distributions $\sum_{i=1}^N \mathbf{a}_i x_i$, $\sum_{i=1}^N \mathbf{o}_i x_i$, and $\sum_{i=1}^N \mathbf{c}_i x_i$ for all videos.

Finally, we want the test set to contain as many as possible interactions, object classes, and diverse object locations to fully evaluate the models. To this end, we calculate the variances $Var\left(\sum_{i=1}^N \mathbf{a}_i x_i\right)$ and $Var\left(\sum_{i=1}^N \mathbf{o}_i x_i\right)$ of interaction and object class distributions, use the variances as minimization objectives to search the suitable videos with the highest varieties of interaction and object classes. Moreover, we find that many objects are located at the half bottom of frames. Thus, to increase the variety of object location, we restrict the distribution of the top half part of heatmaps $\sum_{i=1}^N \sum_{k=1}^{N_h/2} \mathbf{c}_{i,k} x_i$ to a given threshold γ . Additionally, to preserve the frequencies of some interaction classes from degrading to zero, we also add external restrictions on \mathbf{a}_i with a threshold α_j for each interaction class j . The final

Split	Box	Tracklet	Frame
train	234K	104K	102K
test	56K	22K	29K
all	290K	126K	131K

Table 3: Statistics of data split.

programming problem to be solved is

$$\begin{aligned} \min \quad & z = Var\left(\sum_{i=1}^N \mathbf{a}_i x_i\right) + Var\left(\sum_{i=1}^N \mathbf{o}_i x_i\right) \\ \text{s.t.} \quad & x_i \in \{0, 1\}, \quad 1 \leq i \leq N \\ & \sum_{i=1}^N x_i = N_t, \\ & \sum_{i=1}^N \mathbf{a}_{i,j} x_i \geq \alpha_j, \\ & \sum_{i=1}^N \sum_{k=1}^{N_h/2} \mathbf{c}_{i,k} x_i \geq \gamma. \end{aligned}$$

At last, the results are used to select the videos for our test split.

A.2. Statistics of Data Split

The detailed statistics of the data split are shown in Tab. 3.

A.3. Data Samples

Some data samples of DIO are shown in Fig. 7. Human and object GT boxes are in blue and red respectively.

A.4. Interaction List

The detailed interaction classes are listed in Tab. 4.

A.5. Object Class Taxonomy

To deal with the diversity of object class annotations in DIO, following EPIC-Kitchens [11], we use WordNet [54] to construct an object class tree. The detailed procedure is as follows:

- First, with the annotated object class list $W = \{w_1, w_2, \dots\}$, we follow the clustering procedure of Algorithm 1 to build a cluster list C .
- Then, we find some object classes are wrongly clustered due to the polysemy. For example, the first explanation of “banana” in WordNet is a kind of “herb”, instead of “fruit”. For these classes, we manually remove them from C , correct their explanations and add them to C as unique clusters.
- Finally, we follow Algorithm 2 to construct the object class tree with the clusters from C and correct the ambiguous class names.



Figure 7: Data samples and their ST-HOI labels.

Action Id	Action Class	Action Id	Action Class	Action Id	Action Class	Action Id	Action Class
1	jump/leap	14	dress/put on clothing	27	paint	40	shoot
2	lie/sleep	15	drink	28	play board game	41	shovel
3	sit	16	drive	29	play musical instrument	42	smoke
4	answer phone	17	eat	30	play with pets	43	stir
5	brush teeth	18	enter	31	point to	44	take a photo
6	carry/hold	19	exit	32	press	45	text on/look at a cellphone
7	catch	20	extract	33	pull	46	throw
8	chop	21	fishing	34	push	47	touch
9	clink glass	22	hit	35	put down	48	turn
10	close	23	kick	36	read	49	watch
11	cook	24	lift/pick up	37	ride	50	work on a computer
12	cut	25	listen	38	row boat	51	write
13	dig	26	open	39	sail boat		

Table 4: Interaction class list of DIO.

Algorithm 1: Clustering object classes.

Input: object class list $W=\{w_1, w_2, \dots\}$
Output: cluster list $C=\{C_1, C_2, \dots\}$
 Initialize empty cluster list C ;
for $i=1:|W|$ **do**
 if $|C| > 0$ **then**
 for $j=1:|C|$ **do**
 Get $\hat{w}_j \in C_j$ with highest WordNet
 level;
 if WordNet has path between (w_i, \hat{w}_j)
 then
 Add w_i to C_j ;
 else
 Add w_i as a new cluster to C ;
 end
 end
else
 Add w_i as a new cluster to C ;
end
 $i++$;
end

Following the same procedure, we compare the class hierarchies, i.e., the ratio of different word levels in WordNet of DIO with the mainstream video datasets EPIC-Kitchens [11] and Action Genome [29]. The results in Fig. 8 show that our DIO is more complex in classes and thus more challenging.

A.6. Statistics of Action, Object, and Tracklet Length

We also provide the distribution of action, object and tracklet length of DIO in Fig. 9-11.

A.7. Video Clip Duration

The statistics are shown in Fig. 12.

Algorithm 2: Constructing object class tree.

Input: cluster list $C=\{C_1, C_2, \dots\}$
Output: object class tree T
Function ConstructTree(C_i):
 // Construct object class tree T
 from cluster C_i .
 Initialize T from the first word w_1 of C_i ;
for $j=2:|C_i|$ **do**
 Get the j -th word $w_{i,j}$ of cluster C_i ;
 Get the node $T_k \in T$ with the shortest path
 between $(w_{i,j}, T_k)$ in WordNet;
 Add $w_{i,j}$ to T_k ;
end
return T
Function CombineTree(T_x, T_y):
 // Combine object class tree T_x
 and T_y .
 Find root nodes R_x and R_y of T_x and T_y ;
 Find closest common parent R_{xy} of R_x and R_y
 in WordNet;
 Add R_x and R_y to the children of R_{xy} ;
 Construct new class tree T_{xy} from R_{xy} ;
return T_{xy}
 Initialize object class tree $T=\text{ConstructTree}(C_1)$;
for $i=2:|C|$ **do**
 $T_i = \text{ConstructTree}(C_i)$;
 $T = \text{CombineTree}(T, T_i)$;
end

B. Detailed Model Structure

Encoder-Decoder. For each branch of HPN, we adopt an encoder-decoder structure. The detailed structure is presented in Tab. 5.

Condition Module. The condition module of HPN is detailed in Tab. 6. The inputs for the human part and human

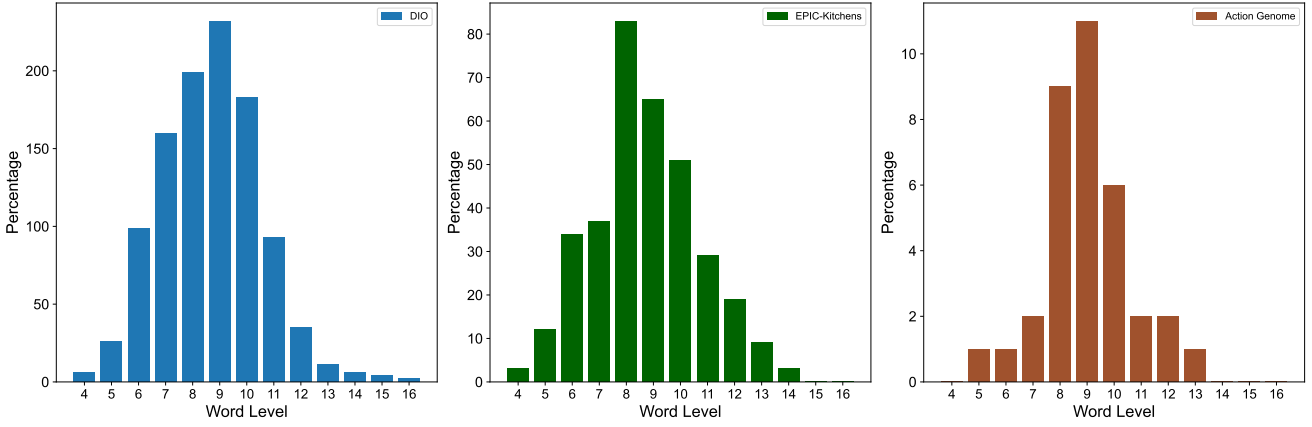


Figure 8: Comparison of object taxonomy between the datasets.

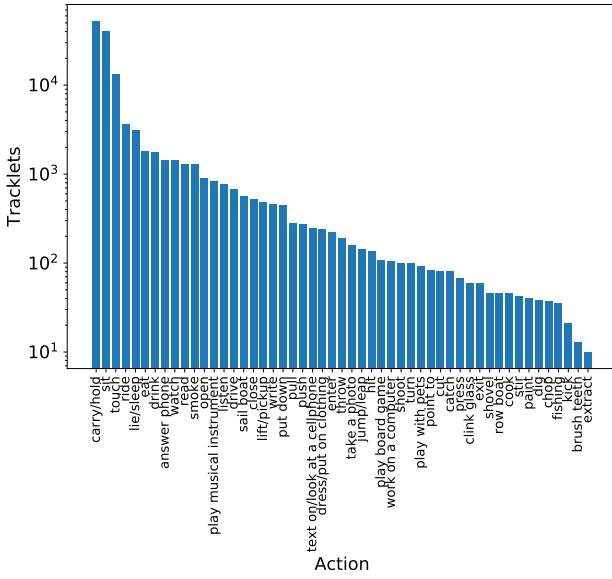


Figure 9: The distribution of tracklet number per action.

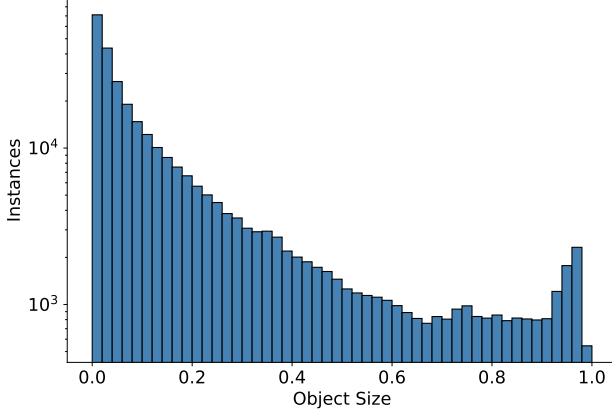


Figure 10: The distribution of normalized object size.

branches are both human appearance feature f_h^k and verb

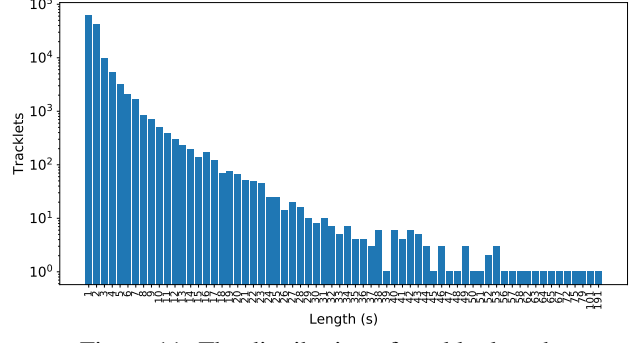


Figure 11: The distribution of tracklet length.

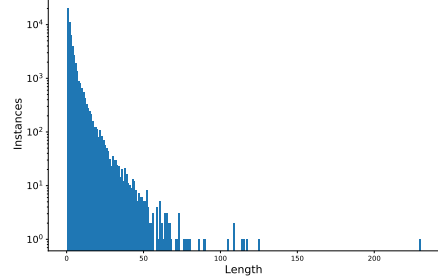


Figure 12: The statistics of temporal duration (second) in DIO.

vector f_v^i . For the context branch, we additionally input the whole frame visual feature f_c^k with f_h^k, f_v^i . The input size of our condition module is unified 4,608, and we use a zero vector to mask the context part of the visual condition for the human part and human branches.

Keypoint maps reweighting. For the reweighting of M_P^k , we first perform Global Average Pooling (GAP) on f_h^k and concatenate it with f_v^i . Then, we input the concatenated conditions to an MLP-Sigmoids layer to generate 18 attention values to reweight the 18 keypoint maps. The detailed structure is presented in Tab. 7.

Stage	Layers	Output Size
	Input Layer	$C_{in} \times 56^2$
Encoder	Conv, (64, 3, 2, 1)	64×28^2
	Conv, (128, 3, 2, 1)	128×14^2
	Conv, (256, 3, 2, 1)	256×7^2
Decoder	Deconv, (256, 3, 2, 1)	256×13^2
	Deconv, (128, 3, 2, 1)	128×25^2
	Deconv, (64, 3, 2, 1)	64×49^2
	Deconv, (32, 3, 2, 1)	32×97^2
	Deconv, (16, 3, 2, 1)	16×193^2
Regression Head	Conv, (51, 1, 1, 0)	51×193^2
	Sigmoid	51×193^2

Table 5: The detailed structure of the encoder-decoder used in our model. The layers are presented in (channels, kernel size, stride, and padding) format. $C_{in} = 20, 2, 77$ for the part, human, and context branches of HPN individually.

Stage	Layers	Output Size
	Visual Input Layer	4608×7^2
Visual Condition	Conv, (1024, 1, 1, 0)	1024×7^2
	Conv, (1024, 1, 1, 0)	1024×7^2
	Global Average Pooling	1024
	Semantic Input Layer	768
Semantic Condition	FC, 392	392
	V+S Concatenation	1416
Condition Decoder	FC, 256	256
	FC, 256	256
	Sigmoid	256

Table 6: The detailed structure of condition module. The convolutional layers are presented in (channels, kernel size, stride, and padding) format. For fully-connected layers, we only present their output dimensions. V+S means visual and semantic.

Stage	Layers	Output Size
	Visual Input Layer	2304×7^2
	Global Average Pooling	2304
	Semantic Input Layer	768
Semantic Condition	FC, 392	392
	V+S Concatenation	2696
Reweighting	FC, 1024	1024
	FC, 18	18
	Sigmoid	18

Table 7: The detailed structure of keypoint maps reweighting. V+S means visual and semantic.

Dynamic Fusion. For dynamic fusion, we concatenate $\hat{M}_P^k, \hat{M}_H^k, \hat{M}_C^k$ and input them into an FC-Softmax to generate dynamic fusion factors $\beta_P, \beta_H, \beta_C$, then $h^{ki} = \beta_P h_P^{ki} + \beta_H h_H^{ki} + \beta_C h_C^{ki}$. The detailed structure is presented in Tab. 8.

Long-term Module. The long-term module used in our model is also an encoder-decoder structure, with a 3D non-

Stage	Layers	Output Size
	Input Layer	768
Dynamic Fusion	FC, 256	256
	FC, 3	3
	Softmax	3

Table 8: The detailed structure of dynamic fusion.

local layer and a temporal pooling layer after the encoder. The detailed structure is presented in Tab. 9.

Stage	Layers	Output Size
	Input Layer	$(2 + N_p) \times (2\tau + 1) \times 56^2$
Encoder	3D Conv, (64, 3, (1, 2), 1)	$64 \times (2\tau + 1) \times 28^2$
	3D Conv, (128, 3, (1, 2), 1)	$128 \times (2\tau + 1) \times 14^2$
	3D Conv, (256, 3, (1, 2), 1)	$256 \times (2\tau + 1) \times 7^2$
	3D Non-local	$256 \times (2\tau + 1) \times 7^2$
	Temporal Average Pooling	256×7^2
Decoder	2D Deconv, (256, 3, 2, 1)	256×13^2
	2D Deconv, (128, 3, 2, 1)	128×25^2
	2D Deconv, (64, 3, 2, 1)	64×49^2
	2D Deconv, (32, 3, 2, 1)	32×97^2
	2D Deconv, (16, 3, 2, 1)	16×193^2
Regression Head	2D Conv, (51, 1, 1, 0)	51×193^2
	Sigmoid	51×193^2

Table 9: The detailed structure of the long-term module. For 2D convolution, the layers are presented in (channels, kernel size, stride, and padding) format. For 3D convolution, the format is (channels, kernel size, (temporal stride, spatial stride), and padding).

Object Size Classifier. For the structure of the object size classifier, we use a two-layer MLP classifier with Softmax. The input of the classifier is the concatenation of f_c^k and f_h^k . For the object of the k -th second and i -th interaction, it would predict its size class. The detailed structure is presented in Tab. 10.

Moreover, we use ReLU as the activation function and BatchNorm with a momentum of 0.9 after each convolutional and fully-connected layer in the modules presented above.

C. Baseline Details

In this section, we supplement some details of the baselines adopted in the experiment.

Proposal Selection [65]. With the RPN [58] finetuned on our train set, we can obtain the proposals of each frame in an ST-HOI tracklet. Naturally, we can directly select one as the predicted object. Given the detected human and proposals, we extract their features f_h^k, f_p^k and the context feature f_c^k . Next, f_h^k, f_p^k are concatenated with f_c^k and fed into an MLP interaction classifier trained with BCE loss. The more accurate a proposal, the better interaction classification it should provide. Thus, for a_i , the proposal with the highest score (performing best on the classification of a_i) is selected.

Stage	Layers	Output Size
Input Layer		4608
Object Size Classifier	FC, 1024	1024
	FC, 153	153
	Reshape	51×3
	Softmax	51×3

Table 10: The detailed structure of object size classifier.

Proposal + Tracking-By-Detection (TBD). Tracking-By-Detection [78] provides a temporal association paradigm to adjust the proposal location on each second. Following MOT methods [53, 59, 80, 3, 71], we use Hungarian algorithm to match the proposals of the nearest two frames, and the Euclid distance matrix between proposal shape vectors $\{x, y, w, h\}$ is used as the cost matrix. The mean interaction score (similar to the baseline proposal selection) of all proposals within a proposal tracklet is used as the tracklet score, the one with the highest mean score is chosen as the prediction.

Proposal + Single Object Tracking (SOT). Another way to adjust the proposal locations temporally is SOT. We adopt SiamRPN [36] with AlexNet backbone as the tracker, input the proposals of the first frame and keep tracking until the final frame. In this way, for each human tracklet we will get the proposal object tubes with the same number of object proposals in one second. For all proposal tracklets, we use the interaction scores of their first frames to select the object predictions. After choosing the object tracklet with the highest prediction score, we can generate a continuous prediction of ST-HOIs. To stabilize the tracking results, in each second of one tracklet, we choose one proposal with the highest IoU to tracked box and directly use it as the tracking result.

Proposal Adjustment [8]. For the proposal with the highest objectness score, we learn an offset between proposal p and GT box o , *i.e.*, $\delta = \{\frac{x_o - x_p}{w_p}, \frac{y_o - y_p}{h_p}, \log \frac{w_o}{w_p}, \log \frac{h_o}{h_p}\}$. Then, we concatenate f_h^k , f_p^k , and f_c^k and input them to an MLP regression head with two FCs. Following object detection, we use a smooth L1 loss to train it.

Human-to-Object [25]. Following [25], we adjust the human box to the object box via an offset. This is in line with our human perspective. For example, when the person is *sitting* or *riding* an object, the location of this interacted object is often under the person. With f_h^k and f_c^k , we use a regression head same with proposal adjustment to learn δ . We use the action feature as input and add the same regression head which we designed for proposal adjustment after the action backbone. Then, we calculate the ground-truth offset between the human and object, *i.e.*, $\delta_{ho} = \{\frac{x_o - x_h}{w_h}, \frac{y_o - y_h}{h_h}, \log \frac{w_o}{w_h}, \log \frac{h_o}{h_h}\}$. Smooth L1 loss is also employed. In testing, we adjust the tracked human box to recover the object location from the predicted offset $\hat{\delta}$.

Another similar way is to learn the offsets between human pose key points and object box [76]. But it performs worse than the box adjustment on val set, thus we report the former implementation.

Density estimation [25]. We can also use the predicted object location as a selection condition for proposals. The original implementation of [25] sees object discovery as density estimation. Given the offsets $\delta_{p|h}$ and $\delta_{o|h}$ from our method, density estimation use a Gaussian function to estimate the likelihood $p_o = e^{-\|\delta_{p|h} - \delta_{o|h}\|^2/2\sigma^2}$ that object locates in the predicted box. Compared to the inference of HPN, density estimation introduces a multiplication between p_o and interaction score S_a^k , to take both action and object location into account.

Heatmap [32]. Recent anchor-free object detectors [83, 35, 67] have shown the capability of objectiveness heatmap to predict the object location distribution. We can also use heatmap estimation to localize objects similar to [32] and HPN. Differently, we direct input the video cues to the model to estimate the heatmap [32]. With the human skeleton map, we first use two convolution layers to extract its feature. Then we concatenate it with f_v^k and f_h^k and input them into a decoder to estimate the heatmap. In testing, the normalization, and filtering with the same threshold of HPN are operated for the heatmap. And the tightest box of the binary mask is adopted as the predicted box.

Box Regression. A pure regression without the help of proposals is also considered. We input the concatenated f_h^k and f_c^k into two FCs with a subsequent ReLU activation and output $\{x, y, w, h\}$ as the location. This simple model is trained with a smooth L1 loss between $\{x, y, w, h\}$ and the GT box. For the test stage, we directly output the predicted object boxes through the network.

D. Detailed Ablation Study

We compare the object discovery performance of HPN on the validation set with different losses, fusion policies, conditions, proposal numbers, and long-term ranges. We report the results in loose 2D and loose 3D metrics. The detailed results are shown in Tab. 11-15.

Loss Function	mIoU(%)	
	Loose 2D	Loose 3D
BCE	30.6	32.2
Smooth L1	25.0	26.3
L2	27.8	29.2

Table 11: The influence of different loss functions.

E. Visualized Object Discovery Results

In Fig. 13, we compare predicted boxes with GT boxes on the test set given GT human tracklets. HPN robustly es-

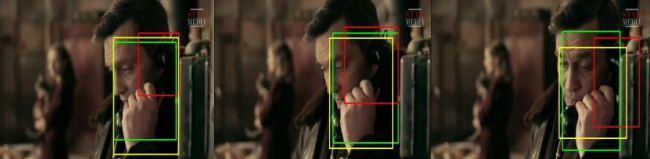
Action	GT HOI Pair	Predicted Object Boxes
Carry/hold		
Answer Phone		
Play Music Instrument		
Sit		
Lie/sleep		
Write		
Ride		
Drink		

Figure 13: Visualizations of interacted object discovery. Boxes: human (blue), GT (green), HPN (yellow), DE(red).

Fusing Policies	mIoU(%)	
	Loose 2D	Loose 3D
Dynamic Fusing	34.2	35.9
Equal Late Fusion	31.1	32.9
Prediction Selection	33.6	35.2

Table 12: The influence of different fusing policies.

Condition	mIoU(%)	
	Loose 2D	Loose 3D
Attention	30.6	32.2
Concatenation	29.6	31.1

Table 13: The influence of different condition translations.

Proposal Number N_p	mIoU(%)	
	Loose 2D	Loose 3D
$N_p = 50$	30.4	32.1
$N_p = 75$	30.6	32.2
$N_p = 100$	30.4	32.1

Table 14: The influence of different proposal numbers.

Long-term Range τ	mIoU(%)	
	Loose 2D	Loose 3D
$\tau = 2$	26.7	27.9
$\tau = 3$	25.0	26.1
$\tau = 4$	25.2	26.3

Table 15: The influence of different long-term ranges. Note that we **only** evaluate the performance of the long-term module instead of the whole model in this experiment.

timates reasonable object locations for various interactions. A video visualization is also provided in the **demo.mp4** file in the supplementary folder.

F. Testing with Ground-truth Inputs

We measure the **upper bound** of object discovery by inputting **ground-truth human boxes and action labels**. The results under two modes are reported: GT human boxes only (H only) and GT human boxes with action labels (H+A). The results are detailed in Tab. 16 and Tab. 17. We can find that under both scenarios, HPN also shows great superiority compared to all baselines. Moreover, given the same GT human tracklets, the advantage of DE has been weakened.

Methods	Interaction Detection (mAP(%))		Object Discovery (mIoU(%))			
	2D	3D	Strict		Loose	
			2D	3D	2D	3D
Proposal Selection (PS)	18.1	13.9	8.4	8.0	20.9	22.2
Proposal + TBD (PTBD)	18.1	13.8	8.8	8.4	21.8	23.3
Proposal + SOT (PSOT)	18.2	13.9	8.2	7.8	20.9	22.3
Proposal Adjustment (PA)	18.0	13.9	10.7	10.4	25.1	26.9
Human-to-Object (HTO)	19.0	14.8	11.9	11.5	28.6	30.7
Density Estimation (DE)	19.3	14.3	11.8	11.4	31.9	34.5
Shortest Distance (SD)	17.9	13.7	11.1	10.7	27.5	29.5
HeatMap (HM)	18.1	14.1	11.3	10.9	27.5	29.5
Box Regression (BR)	17.5	13.7	8.4	8.1	19.2	20.6
HPN-P	18.6	14.7	10.9	10.5	30.8	33.1
HPN-H	18.6	14.4	10.3	9.9	29.7	31.9
HPN-C	19.0	14.9	12.8	12.4	33.8	36.2
HPN	19.7	14.7	13.0	12.5	37.0	39.7

Table 16: ST-HOI learning results with **ground-truth human tracklets** as inputs.

Methods	Object Discovery (mIoU(%))
Proposal Selection (PS)	23.0
Proposal + TBD (PTBD)	23.9
Proposal + SOT (PSOT)	23.2
Proposal Adjustment (PA)	25.6
Human-to-Object (HTO)	28.7
Density Estimation (DE)	32.8
Shortest Distance (SD)	27.8
HeatMap (HM)	28.2
Box Regression (BR)	19.4
HPN-P	31.8
HPN-H	30.4
HPN-C	34.6
HPN	37.8

Table 17: ST-HOI learning results with **ground-truth human tracklets and action labels** as inputs.